THESIS FOR THE DEGREE OF LICENTIATE OF ENGINEERING

Axial phonons and Their Role in Magnetism

NATALIA SHABALA

Department of Physics

CHALMERS UNIVERSITY OF TECHNOLOGY

Göteborg, Sweden 2025

Axial phonons and Their Role in Magnetsim

NATALIA SHABALA

© Natalia Shabala, 2025

Department of Physics Chalmers University of Technology se-412 96 Göteborg, Sweden Telephone +46 (0)31 772 10 00

Cover: Ions on a crystal lattice moving in circular orbits and thus inducing magnetization of the material.

Chalmers digitaltryck Göteborg, Sweden 2025

Axial phonons and Their Role in Magnetsim

NATALIA SHABALA

Department of Physics

Chalmers University of Technology

Abstract

Phonons are collective lattice excitations that can be understood as quantized modes of vibration. In recent years, it has been shown that a particular kind of phonons, namely axial phonons, or circularly polarized phonons, can induce magnetization of the material. Excitingly, experimental evidence has shown that the arising magnetization is unexpectedly large. Understanding this phenomenon has been an active topic of research in recent years.

This thesis presents the contributions to this area based on two papers. The first paper presents a microscopic theory for magnetization induced by axial phonons. This theory is based on treating the interaction between the phonons and the electrons as a second order perturbation of the system. The second paper reviews the recent progress of the field. Here, the concept of axial phonons is introduced alongside with the phenomenological arguments for emergent magnetization. A summary of the experimental observations of the magnetization induced by axial phonons is also provided. Additionally, an overview of recently proposed microscopic theories of the effect is presented. Finally, in an additional chapter the perspective of observing the effect of axial phonons on other physical phenomena, such as the conventional and the anomalous Hall effect, is discussed.

Keywords: Lattice vibrations, axial phonons, circularly polarized phonons, magnetism, inverse Faraday effect, electron-phonon coupling

LIST OF APPENDED PAPERS

This thesis is based on work presented in the following papers:

I Phonon inverse Faraday effect from electron-phonon coupling Natalia Shabala and R. Matthias Geilhufe Physical Review Letters 133, 266702 (2024)

II Axial phono-magnetic effects

Natalia Shabala, Finja Tietjen, and R. Matthias Geilhufe *In manuscript*

The author's contribution to the papers:

- I Contributed to the derivation of the effective Hamiltonian, generated the plots comparing theoretical predictions with experimental results, and drafted substantial portions of the manuscript.
- II Wrote several sections of the review paper and participated actively in the revision process.

Contents

vii

Li	st of a	bbreviations	ix
1	Intr	oduction	1
2	Role	of electrons in phono-magnetic effects	5
	2.1	Phonons as collective lattice displacement	5
	2.2	Landau theory	7
	2.3	Dynamical multiferroicity	8
	2.4	Experimental evidence	10
	2.5	Role of electrons in phono-magnetic effects	11
3	Pho	non inverse Faraday effect	15
	3.1	Optical inverse Faraday effect	15
	3.2	Phonon inverse Faraday effect	17
	3.3	Effective magnetic field in $SrTiO_3$	20
4	Axia	al phonons and (anomalous) Hall effect	27
	4.1	Real vs effective magnetic field	27
	4.2	Hall effect and Anomalous Hall effect	28
	4.3	The setup	30
	4.4	Magnetic field and transverse resistivity calculation	31
5	Sum	mary of papers	35
6	Con	clusion and outlook	37
	6.1	Conclusion	37
	6.2	Outlook	38
Ad	know	ledgments	41
Bi	bliogi	raphy	43

Papers I–II 47

Introduction

Phonons are collective excitations of the crystal lattice that can be understood as wave packets of atomic vibrations [1], and can therefore be treated as quasiparticles. They are typically described in terms of the displacement of atoms from their equilibrium positions. This thesis focuses on a particular kind of phonons in which the atoms move in a circular trajectory. Such phonon modes, known as circularly polarized or axial phonons, are distinguished by their nonzero angular momentum.

Circularly polarized phonons have recently become an active area of research because of their ability to induce magnetization even in materials without preexisting magnetism due to electronic spin, as illustrated in Fig. 1.1. Thus, axial phonons open a new way of influencing and controlling magnetic properties of a material, which has

Magnetization

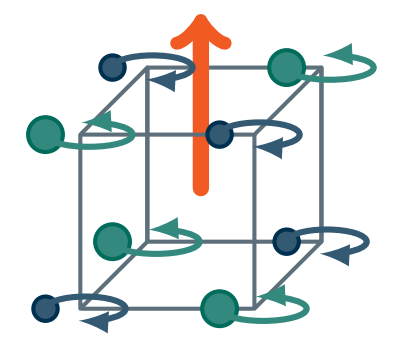


Figure 1.1: Schematic illustration of circularly polarized (axial) phonons represented by collective vibrations in which the atoms move in circular orbits. The resulting magnetization is shown as an upwards arrow.

potential applications in data storage and processing and spintronics. However, in order to utilize this potential, there needs to be a reliable way of predicting the size of the emergent magnetization.

The arising magnetization can be explained by the fact that a cyclotron motion of a charged particle is expected to result in a magnetic moment, due to the fact that the magnetic moment of a particle is proportional to its angular momentum [2]. Therefore, a simple estimate of the size of the phono-magnetic effects can be made through the gyromagnetic ratio, i.e., the proportionality constant between the angular momentum and the resulting magnetic moment. The gyromagnetic ratio is largely determined by the mass of the particle. For a mass of an ion, an estimate based on the gyromagnetic ratio gives a magnetic moment on a scale of $10^{-6}\mu_{\rm B}$.

However, this estimate does not agree with the experimental observations. Recently, a number of experiments have been conducted to detect and measure the resulting magnetization [3–18]. A common thread that links these observations is that they report a magnetic moment several orders of magnitude larger than what the gyromagnetic ratio would indicate. This highlights a gap in the understanding of phono-magnetic effects. Evidently, the cyclotron motion of a charged particle cannot fully explain the magnetization arising from circularly polarized phonons. However, what other factors contribute to this magnetization remains unclear. This thesis explores this topic by attempting to answer the following questions:

- Apart from ionic motion, what other effects contribute to the phonomagnetic effects resulting in the large magnetization observed experimentally?
- How can we better understand the nature of the magnetization induced by axial phonons and how does it affect other physical phenomena such as the Hall effect?

To address these questions, we first provide background information on phonons in Chapter 2. Furthermore, in this chapter we phenomenologically motivate the connection between phonon angular momentum and magnetization. We proceed to give an overview of the experimental evidence that suggests that this magnetic moment reaches large values. Finally, we give an argument for investigating the role of electrons in phono-magnetic effects. In Chapter 3, we introduce a formalism for explaining and predicting phonon-induced magnetization, which is based on time-dependent perturbation theory and electron-phonon coupling. In our formalism, we consider the effect as the phonon analogue to the optical inverse Faraday effect. Further, in Chapter 4, we explore the second question presented above, investigating the possibility of using conventional and anomalous Hall effects to understand the nature of the effective magnetic field induced by axial phonons. We also present a summary of the papers

included in Chapter 5. Finally, we conclude the thesis in Chapter 6.

This work is based on the two attached papers. Paper I and II deal with the first question. Paper I proposes a new microscopic theory for the magnetization arising from axial phonons presented in Chapter 3, while Paper II reviews recent progress in the field, outlined in Chapter 2. The second question is addressed in Chapter 4, which explores the possibilities of extending and verifying the progress outlined in Paper II.

Role of electrons in phono-magnetic effects

In this chapter, we first introduce the key concepts related to phonons in section 2.1 and then proceed to motivate, from a phenomenological perspective, the contribution of axial phonons to magnetization. To provide this motivation, we first discuss the emergent magnetization in terms of Landau theory in section 2.2. In section 2.3 we then explain the connection between circularly polarized phonons and magnetization in terms of dynamical multiferroicity, i.e., a phenomenon in which a time-varying electric polarization induces magnetism in an otherwise non-magnetic material [19]. We proceed to outline the experimental observations of phono-magnetic effects in section 2.4. As noted in Chapter 1, the observed magnetization is significantly larger than previously expected. Finally, in section 2.5, we argue that the interaction between electrons and phonons may explain the large magnetization, which motivates the further direction of this thesis.

2.1 Phonons as collective lattice displacement

As mentioned in the introductory chapter, phonons are collective crystal lattice excitations. They can be described by the displacement τ of individual atoms from their equilibrium positions:

$$\boldsymbol{\tau}_{pj} = \boldsymbol{R}_{pj} - \boldsymbol{R}_{pj}^{0}. \tag{2.1}$$

Here, p denotes the unit cell in the crystal and j an atom in the unit cell. To study phonons, it is convenient to use the harmonic approximation which involves Taylor expanding the total potential energy U up to the second order around the equilibrium

positions of the atoms [20]:

$$U = U^{0} + \sum_{pj\alpha} \frac{\partial U(\tau^{0})}{\partial \tau_{pj\alpha}} \tau_{pj\alpha} + \sum_{\substack{pj\alpha \\ p'j'\alpha'}} \frac{\partial U(\tau^{0})}{\partial \tau_{pj\alpha} \partial \tau_{p'j'\alpha'}} \tau_{pj\alpha} \tau_{p'j'\alpha'}. \tag{2.2}$$

Here, α denotes the Cartesian direction. The second term contains the first derivative of the potential energy with respect to position, which can be recognized as the force, $\partial U(\tau^0)$

 $F_{pj\alpha}\left(\boldsymbol{\tau}^{0}\right)=-\frac{\partial U\left(\boldsymbol{\tau}^{0}\right)}{\partial \tau_{pj\alpha}}$. Assuming that at the equilibrium position $\boldsymbol{\tau}^{0}=0$ there are no external forces acting on the atoms, we can set the second term to zero. This way to define force also allows us to rewrite the classical equation of motion as:

$$m_{pj}\ddot{\tau}_{pj} = -\sum_{p'j'\alpha'} C_{pj\alpha,p'j'\alpha'} \tau_{p'j'\alpha'}, \qquad (2.3)$$

where $C_{pj\alpha,p'j'\alpha'}$ is a force constant matrix, which is defined as

$$C_{pj\alpha,p'j'\alpha'} = \sum_{\substack{pj\alpha\\p'j'\alpha'}} \frac{\partial U(\tau^0)}{\partial \tau_{pj\alpha}\partial \tau_{p'j'\alpha'}}.$$
 (2.4)

Assuming that the solutions to Eq. (2.3) have the form of plane waves allows to rewrite Eq. (2.3) in the form of an eigenvalue problem:

$$\sum_{i'\alpha'} D_{j\alpha,j'\alpha'}(q) \xi_{j'\alpha',\nu}(q) = \omega_{q\nu}^2 \xi_{j\alpha,\nu}(q), \qquad (2.5)$$

where $D_{i\alpha,i'\alpha'}(q)$ is the dynamical matrix, defined as

$$D_{j\alpha,j'\alpha'}(q) = \frac{1}{\sqrt{m_j m_{j'}}} \sum_{p} C_{0j\alpha,pj'\alpha'} \exp(iq \cdot \mathbf{R}_p), \tag{2.6}$$

with q denoting the quasimomentum. The dynamical matrix is Hermitian, and therefore its eigenvalues are real. Specifically, its eigenvalues are the phonon frequency modes $\omega_{q\nu}$, which can be obtained from the eigenvalue problem in Eq. (2.5). The eigenvectors $\xi_{j\alpha,\nu}(q)$ are commonly referred to as phonon polarization vectors. The polarization vectors are orthonormal [20]:

$$\sum_{\nu} \xi_{j'\alpha',\nu}^{*}(q) \, \xi_{j\alpha,\nu}(q) = \delta_{jj'} \, \delta_{\alpha\alpha'},$$

$$\sum_{i\alpha} \xi_{j\alpha,\nu}^{*}(q) \, \xi_{j\alpha,\nu'}(q) = \delta_{\nu\nu'}.$$
(2.7)

For each ion j, Eq. (2.5) gives us a set of eigenvalues and eigenvectors denoted by v, which also depend on the quasimomentum q. The different eigenvalues correspond to the distinct phonon frequency modes, ω_{qv} . Since we applied the harmonic approximation, we can now view each phonon mode as an independent harmonic oscillator with frequency ω_{qv} [20].

Phonon modes can be classified as linear (e.g., optical or acoustical) or circularly polarized, which are also referred to as axial phonons. This thesis focuses primarily on the latter variety, which is defined as a phonon with a non-zero phonon angular momentum:

$$L_{\rm ph} = \mathbf{u} \times \dot{\mathbf{u}}.\tag{2.8}$$

Here, instead of displacement τ , phonon normal coordinates are used. They are defined as $u_{pj} = \sqrt{m_{pj}} \tau_{pj}$.

2.2 Landau theory

Magnetization arising from circularly polarized phonons can be motivated phenomenol-gically through the use of free energy [21]. In order to do that, we consider two degenerate linearly polarized phonon modes labeled by μ and ν . The degeneracy allows us to introduce a basis transform from $\{u_{\mu}, u_{\nu}\}$ to a circularly polarized basis, $\{u_{R}, u_{L}\}$. In this new basis, the displacement can be written as

$$\boldsymbol{u}(t) = \left(\frac{1}{\sqrt{2}}u_R(\hat{\boldsymbol{e}}_{\mu} + i\hat{\boldsymbol{e}}_{\nu}) + \frac{1}{\sqrt{2}}u_L(\hat{\boldsymbol{e}}_{\mu} - i\hat{\boldsymbol{e}}_{\nu})\right)e^{i\omega_{\mathrm{ph}}t},\tag{2.9}$$

with $u_R = (u_\mu - iu_\nu)/\sqrt{2}$ and $u_L = (u_\mu + iu_\nu)/\sqrt{2}$. With the displacement defined by Eq. (2.9) we can define the free energy function as

$$F_u = \chi B_z (u_R u_R^* - u_L u_L^*) = i \chi B_z (u_\mu u_\nu^* - u_\nu u_\mu^*), \tag{2.10}$$

where B_z is the component of the magnetic field perpendicular to the plane of the phonon modes μ and ν . Here, we have used the symmetry criteria of a nonmagnetic and inversion symmetric crystal. Namely, for such a crystal the thermodynamic free energy has to be even under time reversal and space inversion. Since the displacement is odd under space inversion and even under time reversal, the free energy in Eq. (2.10) fulfills the symmetry criteria. Eq. (2.10) represents the connection between the circularly polarized phonons and the magnetic field. Furthermore, the magnetization can be obtained from the expression of the free energy through:

$$M_{z} = -\frac{\partial F_{u}}{\partial B_{z}} = \chi (u_{L}u_{L}^{*} - u_{R}u_{R}^{*}). \tag{2.11}$$

The equation above describes the relationship between the magnetization and the circularly polarized phonons. In particular, it becomes clear that the imbalance between left- and right-circularly polarized phonons is important, since if $u_L u_L^* = u_R u_R^*$, magnetization becomes zero.

2.3 Dynamical multiferroicity

It is also possible to understand the phonon-induced magnetization by considering the influence of axial phonons on the polarization of the material [19]. In a crystal lattice exhibiting axial phonons, the circular motion of ions is expected to cause magnetization \boldsymbol{M} of the material through the relationship:

$$\boldsymbol{M} \sim \boldsymbol{P} \times \partial_t \boldsymbol{P}.$$
 (2.12)

This relationship describes the concept of dynamical multiferroicity, i.e., magnetization arising from time-varying electrical polarization. To relate Eq. (2.12) to phonons, we note that the polarization P is closely related to the phonon normal modes u. This can be seen by considering the definition of the Born effective charge [22, 23]:

$$Z_{j\alpha\beta} = \Omega_0 \frac{\partial P_\alpha}{\partial u_{j\beta}}. (2.13)$$

Here, Ω_0 is the unit cell volume, while j labels the ions and α and β refer to the Cartesian directions. Rearranging the equation above and integrating both sides gives us

$$P_{\alpha} = \frac{1}{\Omega_0} Z_{j\alpha\beta} u_{j\beta}. \tag{2.14}$$

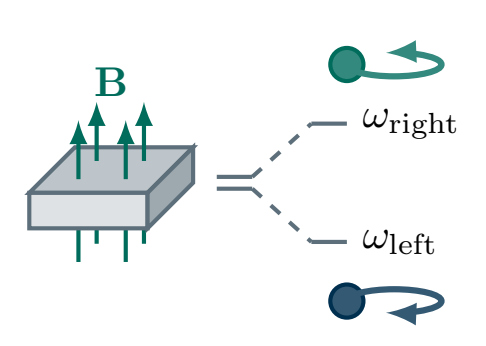
Thus, Eq. (2.12) can be rewritten in terms of the ion displacement:

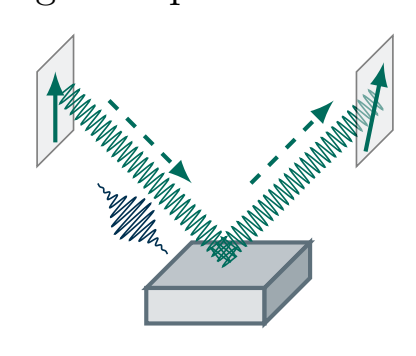
$$\mu_{\rm ph} = \gamma \mathbf{u} \times \dot{\mathbf{u}} = \gamma \mathbf{L}_{\rm ph}. \tag{2.15}$$

Here, instead of the magnetization M, which is defined as the magnetic moment per unit volume [24], we used the phonon magnetic moment $\mu_{\rm ph}$. Eq. (2.15) shows that the magnetic moment arising from phonons is proportional to phonon angular momentum, i.e., the magnetization depends directly on the circular polarization of the phonons. The proportionality constant is the gyromagnetic ratio γ , which is given by $\gamma = \frac{q}{2m}$, where m is the mass of the particle, and q its charge. To approximate the gyromagnetic ratio for an ion, we take the mass of a proton and elementary charge, i.e., $\gamma \approx \frac{1}{2} e \, \mathrm{Da}^{-1}$. To obtain an estimate for the phonon angular momentum, we assume the ionic displacement $|\tau| \approx 0.1 \, \mathrm{\mathring{A}}$ and the phonon frequency of $\omega_{\mathrm{ph}} \approx 2\pi \times 1 \, \mathrm{THz}$, which gives $L_{\mathrm{ph}} \approx 1 \times 10^{-2} \, \hbar$. With the approximate value of the gyromagnetic ratio, we obtain $|\mu_{\mathrm{ph}}| \approx 5.4 \times 10^{-2} \, \hbar$. With the approximate value of the gyromagnetic ratio, we obtain $|\mu_{\mathrm{ph}}| \approx 5.4 \times 10^{-2} \, \hbar$.

Phonon Zeeman effect

Magneto-optical Kerr effect





Magnetic switching



Figure 2.1: Illustration of the phenomena that have been used to detect phono-magnetic effects experimentally. The Phonon Zeeman effect is characterized by the splitting of a phonon mode into left- and right-circularly polarized phonon modes under the influence of an external magnetic field. The magneto-optical Kerr effect demonstrates a rotation of polarization of a linearly polarized field reflected off a magnetized sample. In this case, the magnetization is induced by a circularly polarized pump field driving circularly polarized phonons in the crystal. Magnetic switching shows a permanent reversal of magnetic order with the help of circularly polarized phonons modes driven by a laser.

 $10^{-6}\mu_{\rm B}$. Here it is important to note that this estimate relies on a relatively large ionic displacement of $|\tau|\approx 0.1$ Å. In most cases, root mean square displacement amounts to only a few percent of the interatomic distance, which is typically on the order of an Å. However, in certain materials, the root mean square displacement excited by a laser drive can reach up to 10% of the interatomic distance before the sample is destroyed [25]. Therefore, the value given above should be regarded as an upper bound for the phonon magnetic moment.

To evaluate this estimate, we turn to the existing experimental observations of the phonon magnetic moment.

2.4 Experimental evidence

While the experimental evidence supports the existence of the phonon magnetic moment, various observations report larger magnetization than the estimate presented at the end of section 2.3 which is based on the ionic motion alone. In this section, we give an overview of the experimental observations. The physical phenomena used to detect phonon-induced magnetization are illustrated in Fig. 2.1.

One way to experimentally measure the phonon magnetic moment is through the phonon Zeeman effect, which constitutes a splitting of a degenerate phonon mode into two circularly polarized modes with opposite helicities [19]. This splitting is facilitated by an external magnetic field $\bf \it B$. The size of the splitting, $\Delta \omega$, can be measured through, e.g. Raman spectroscopy. The phonon magnetic moment, $\mu_{\rm ph}$, is then calculated through:

$$\hbar \Delta \omega_{\rm ph} = \boldsymbol{\mu}_{\rm ph} \cdot \boldsymbol{B}. \tag{2.16}$$

The experimental observations recording the phonon Zeeman effect have been performed on various materials. The earliest experiments were conducted on CeF₃ and CeCl₃ and report a Zeeman splitting corresponding to magnetic moments of up to 12.6 $\mu_{\rm B}$ and 21 $\mu_{\rm B}$, respectively [3–5]. More recent experiments involve, for example, MoS₂, where the Zeeman splitting indicates a magnetic moment of 2.5 $\mu_{\rm B}$ [8, 9]. A similar measurement in CoTiO₃ indicates a phonon magnetic moment of up to 1.11 $\mu_{\rm B}$ [10]. Smaller values of the phonon magnetic moment have also been recorded. For example, in PbTe the Zeeman splitting indicates a phonon magnetic moment of $4 \times 10^{-2} \mu_{\rm B}$ [7].

Interestingly, in the ferrimagnet $Fe_{1.75}Zn_{0.25}Mo_3O_8$ the phonon magnetic moment was shown to be dependent on the temperature, reaching a value of 2.62 μ_B near the Néel temperature and 0.22 μ_B in lower temperature regimes [12]. A similar dependency was observed in $Fe_2Mo_3O_8$, where the phonon magnetic moment was increased by a factor of 6 near the Néel temperature [11]. Comparably, in a ferromagnet $Co_3Sn_2S_2$ the phonon magnetic moment exhibits a similar dependency on the Curie temperature [13].

Some measurements were performed using Dirac materials. For example, in the Dirac semimetal Cd_3As_2 the phonon Zeeman splitting indicates a phonon magnetic moment of 2.7 μ_B [6]. In topological materials, such as $Pb_{0.4}Sn_{0.6}Te$, the phonon magnetic moment was shown to depend on the topological phase of the material, increasing by two orders of magnitude at the transition from the trivial to the topological phase and reaching values of up to 3.3 μ_B [15].

Alternatively, phonon-induced magnetization can be observed through the magnetooptical Kerr effect, i.e., rotation of the polarization of a linearly polarized light caused by the reflection off a magnetized sample [26]. To utilize this phenomenon, a pumpprobe setup is used where the sample is driven with a circularly-polarized pump laser field, which drives the phonons inside the crystal, ensuring their circular polarization. Subsequently, the magnetization is measured by observing the polarization rotation of the linearly polarized probe laser field after it reflects from the material. The magnetic moment per unit cell is then proportional to the angle of polarization rotation [16]. In $SrTiO_3$, the phonon magnetic moment observed using this method was reported to be approximately $0.1\mu_B$, which translates into a magnetic field of approximately 32 mT. A similar measurement performed on CeF_3 resulted in an effective magnetic field of 1 T [17], which is significantly larger than in the $SrTiO_3$ experiment from Ref. [16]. However, considering the size of the primitive unit cell in CeF_3 the reported magnetic moment per unit cell only reaches values of $0.003~\mu_B$ [17].

Moreover, axial phonons provide a means to influence the magnetic properties of a material outside the sample, as shown in proximity switching experiments [18]. In such an experimental setup, axial phonons are induced by a circularly polarized pump field. Magneto-optical images of a material placed on top of the sample reveal a switching of magnetic order that depends on the helicity of the pump field. This helicity dependence highlights the role of axial phonons: a right-circularly polarized pump field excites right-circularly polarized ionic motion, thereby determining the direction of the induced magnetization.

Therefore, it can be concluded that circularly polarized phonons give rise to a significant magnetization that can be observed and used for manipulating magnetic properties of a material. However, there is a discrepancy between the values of phonon magnetic moment obtained classically by considering the circular motion of ions and the experimental observations. This shows that these phono-magnetic effects are influenced by other mechanisms, which are not taken into account by calculating the magnetic moment from a cyclotron motion of ions.

2.5 Role of electrons in phono-magnetic effects

In search of the origin of this effect, we start by considering the gyromagnetic ratio again. As mentioned previously, the gyromagnetic ratio is the ratio between the magnetic moment and the angular momentum that is causing it. Therefore, we can express the magnetic moment of an electron as

$$\mu_e = \gamma \hbar = \frac{e}{2m_e} \hbar. \tag{2.17}$$

At the same time, it is known that the magnetic moment of an electron is equal to the Bohr magneton [27], which is closer to the experimentally observed values discussed in section 2.4. This hints at the involvement of electrons in phono-magnetic effects. This direction of describing phono-magnetic effects has been explored by a number of recent theoretical works [21, 28–33]. Theoretical approaches can be divided into three categories: adiabatic, Floquet, and perturbation.

The Floquet approach involves studying the influence of axial phonons on electronic energy levels by using the Floquet perturbation theory [28], which can be applied to systems described by a time-periodic Hamiltonian, i.e., H(t+T) = H(t) [34]. Assuming a coupling between the circularly polarized phonon mode and the electron degrees of freedom, the Hamiltonian becomes time-periodic, allowing the use of Floquet theory. Thus, it can be shown that circularly polarized phonons lead to splitting in the electronic energy levels [28]. By analogy with the Zeeman effect, the size of the splitting is expected to be proportional to the effective magnetic field. With this method, the effective magnetic field is estimated to be of the order of kT [28], which significantly exceeds the magnetic field that can be expected from the phonon magnetic moments observed in the experiments outlined in section 2.4. A potential explanation for this could involve the fact that this magnetic field was calculated at the Γ point in momentum space. Transforming it to real space would require taking an average over the full Brillouine zone, leading to a lower estimate.

Another recently proposed microscopic theory uses the adiabatic approximation to approach the problem. This formalism considers the characteristic circular ionic motion of axial phonons as a source of the adiabatic evolution of the electronic states [29]. The magnetization induced by circularly polarized phonons can thus be related to the Berry curvature hinting at its topological origins. This view on the effect leads to an estimate of the phonon magnetic moment of the order of a Bohr magneton [29].

An alternative approach to the adiabatic and Floquet methods is viewing circularly polarized phonons through the lens of perturbation theory. Similarly to the Floquet approach, this method involves considering a Hamiltonian which involves an additional term that arises from electron-phonon coupling:

$$H = H_0 + H_{\text{el-ph}}.$$
 (2.18)

The Hamiltonian in Eq. (2.18) describes the electronic energy levels, including the effects from the electron-phonon interaction.

Assuming that the displacement of ions is sufficiently small, the effects of $H_{\rm el-ph}$ can be studied using perturbation theory. This can be done through the Green function formalism [30, 31] or by viewing the resulting magnetization as a vibrational analogue to the optical Faraday effect, i.e., the phonon inverse Faraday effect. This approach is described in more detail in Chapter 3.

Even though the theoretical models developed in recent years differ in their approaches to the problem of phono-magnetic effects, all of them are in agreement that electrons play an important role in these effects. Specifically, electron-phonon coupling is particularly important, since several works highlight that the size of the magnetization depends quadratically on its strength [21, 28, 30]. Furthermore, when certain frequency limits are considered, different theoretical approaches correspond well to each other. For example, the Floquet theory method in the high frequency limit gives the

same result as the phonon inverse Faraday effect approach [28]. Similarly, the low frequency limit of the phonon inverse Faraday effect method agrees with the results of the adiabatic approach [21].

Phonon inverse Faraday effect

In the previous chapter, we motivated the need to explain phonon-induced magnetization at the electronic level. Building on this, we propose a microscopic theory of such magnetization based on electron-phonon interactions. This brings us closer to answering the first research question presented in Chapter 1, as we investigate the contributions to phonon-induced magnetism beyond ionic motion alone. Our formalism is based on treating the magnetism induced by circularly polarized phonons as a phonon analogue to the optical inverse Faraday effect, in which the magnetization is induced by circularly polarized light. Thus, the origin of this effect closely mirrors that of circularly polarized phonons. Therefore, we start this chapter by introducing the optical inverse Faraday effect in section 3.1. We proceed to discuss the phonon inverse Faraday effect formalism in section 3.2. In section 3.3 we apply our formalism to estimate the effective magnetic field arising from axial phonons in SrTiO₃.

3.1 Optical inverse Faraday effect

The optical inverse Faraday effect refers to the process of magnetization of a material under the influence of a circularly polarized laser pulse [35, 36]. In this case, the electric field of the laser pulse is given by

$$E(t) = 2\operatorname{Re}\left[\frac{1}{\sqrt{2}}(\hat{\boldsymbol{e}}_{x} + i\hat{\boldsymbol{e}}_{y})\mathcal{E}_{R} + \frac{1}{\sqrt{2}}(\hat{\boldsymbol{e}}_{x} - i\hat{\boldsymbol{e}}_{y})\mathcal{E}_{L}\right]e^{i\omega t},\tag{3.1}$$

where ω is the laser frequency and $\mathcal{E}_{R,L}=\frac{1}{\sqrt{2}}(\mathcal{E}_x\mp i\mathcal{E}_y)$, with \mathcal{E}_x , \mathcal{E}_y denoting the amplitude of the electric field strength in the respective direction. The electric field is thus directed along the z-axis and expected to give rise to a magnetization along

the same direction. The size of this magnetization can be calculated through the same consideration of the free energy as discussed in Chapter 2 [36]:

$$M = -\chi(\mathscr{E}_R \mathscr{E}_R^* - \mathscr{E}_L \mathscr{E}_I^*). \tag{3.2}$$

From the equation above it is clear that the magnetization is expected to depend quadratically on the electric field strength, which echoes closely the phenomenological motivation of the phonon magnetization discussed in Chapter 2. In contrast to phonon-induced magnetization, the magnetization in the optical inverse Faraday effect is induced by the electric field of a circularly polarized laser.

Pershan *et al.* describe the optical inverse Faraday effect using perturbation theory [36], starting from a Hamiltonian in the form:

$$\hat{H} = \hat{H}_0 + V(t), \tag{3.3}$$

where \hat{H}_0 is the unperturbed Hamiltonian and V(t) is the time-dependent perturbation, which is assumed to be small. If the perturbation is time-periodic, it is possible to write it as:

$$V(t) = v(t)e^{i\omega t} + \text{c.c.}, (3.4)$$

where ω is the frequency of the perturbation. The equation above separates the perturbation into two parts: the perturbation amplitude v(t) and a time-dependent component $e^{i\omega t}$. Assuming that the perturbation amplitude varies on a much larger time scale than $\frac{1}{\omega \pm \omega_{ij}}$, with $\hbar \omega_{ij}$ being the energy difference between electronic levels labeled by i and j [37], the effect of the perturbation on the electronic system can be described by an effective Hamiltonian:

$$\langle a|H_{\text{eff}}(t)|b\rangle = -\sum_{n} \left[\frac{\langle a|v|n\rangle\langle n|v^*|b\rangle}{E_{nb} - \hbar\omega} - \frac{\langle a|v^*|n\rangle\langle n|v|b\rangle}{E_{nb} + \hbar\omega} \right], \tag{3.5}$$

which allows one to calculate the overlap elements between electronic states $|a\rangle$ and $|b\rangle$. Here, $|n\rangle$ denotes the unperturbed electronic states while E_{nb} is the energy gap between the respective electronic energy levels.

Assuming that the laser pulse from Eq. (3.1) couples to the system through dipole coupling, the perturbation becomes:

$$V(t) = \operatorname{Re}\left[e\mathbf{r} \cdot \mathscr{E}e^{i\omega t}\right]. \tag{3.6}$$

Thus, the perturbation amplitude takes the form:

$$v(t) = e(r_+ \mathcal{E}_R - r_- \mathcal{E}_L), \tag{3.7}$$

where $r_{\pm} = \frac{1}{\sqrt{2}}(x \mp iy)$. Using Eq. (3.7) in Eq. (3.5) gives the effective Hamiltonian:

$$\langle a|H_{\text{eff}}|b\rangle = e^{2} \left[\mathcal{E}_{R} \mathcal{E}_{R}^{*} - \mathcal{E}_{L} \mathcal{E}_{L}^{*} \right]$$

$$\times \sum_{n} \frac{\hbar \omega}{E_{nb}^{2} - \hbar^{2} \omega^{2}} \left[\langle a|r_{+}|n\rangle \langle n|r_{-}|b\rangle - \langle a|r_{-}|n\rangle \langle n|r_{+}|b\rangle \right].$$
(3.8)

Here, it is important to note that while the expression for the effective Hamiltonian includes other terms, only $\mathscr{C}_R\mathscr{C}_R^*-\mathscr{C}_L\mathscr{C}_L^*$ transforms as a magnetic field, and therefore only the terms containing such an expression will contribute to the magnetization.

Eq. (3.8) describes the effect of the perturbation in the form of circularly polarized light on the electronic levels of the system. This expression can be used to show that $\mathscr{E}_R\mathscr{E}_R^* - \mathscr{E}_L\mathscr{E}_L^*$ acts as a time reversal symmetry breaking field, polarizing the spins as a magnetic field would [36].

3.2 Phonon inverse Faraday effect

To apply the formalism of the optical inverse Farady effect to the case of axial phonons we assume that the Hamiltonian can still be written in the form given by Eq. (3.3), with the perturbation now originating from the displacement of ions. For lattice vibrations such a displacement can be assumed to be sufficiently small, and we are still able to apply perturbation theory. In order to write down the new form of the perturbation, we linearize the potential energy in terms of the atom displacement and write down the perturbation as:

$$V(t) = \sum_{pj\alpha} \frac{\partial U}{\partial \tau_{pj\alpha}} \tau_{pj\alpha}, \tag{3.9}$$

where p denotes a unit cell, j an atom and α is the Cartesian direction of the displacement. At the same time, for a circularly polarized phonon, we can write down the displacement as:

$$\tau = \left(\frac{1}{\sqrt{2}}\tau_R(\hat{\boldsymbol{e}}_{\mu} + i\hat{\boldsymbol{e}}_{\nu}) + \frac{1}{\sqrt{2}}\tau_L(\hat{\boldsymbol{e}}_{\mu} - i\hat{\boldsymbol{e}}_{\nu})\right)e^{i\omega_{\mathrm{ph}}t}.$$
 (3.10)

Here, we rewrite the phonon displacement in the circularly polarized basis where μ and ν denote two perpendicular phonon modes. The displacement amplitudes $\tau_{R,L}$ are given by $\tau_{R,L} = \frac{1}{\sqrt{2}}(\tau_{\mu} \mp i\tau_{\nu})$. The perturbation now takes the form:

$$V(t) = 2\operatorname{Re}\left[\boldsymbol{\tau} \cdot \nabla_{\boldsymbol{\tau}} U e^{i\omega_{\mathrm{ph}}}\right]. \tag{3.11}$$

Thus, we can still write it down in the shape given by Eq. (3.4) and therefore use the effective Hamiltonian in Eq. (3.5). First, we focus on a simplified case and consider a

single ion moving on a circular orbit. Then, the perturbation amplitude from Eq. (3.4) takes on the form:

$$v(t) = \tau_0 \cdot \nabla_{\tau} U, \tag{3.12}$$

where $\tau_0 = \left(\frac{1}{\sqrt{2}}\tau_R(\hat{e}_{\mu} + i\hat{e}_{\nu}) + \frac{1}{\sqrt{2}}\tau_L(\hat{e}_{\mu} - i\hat{e}_{\nu})\right)$. Using this perturbation amplitude in Eq. (3.5), gives us an expression for the effective Hamiltonian:

$$H_{\text{eff}}^{ab} = -\sum_{n} \left[\frac{E_{nb}}{E_{nb}^{2} - \hbar\omega^{2}} \left((\tau_{R}\tau_{R}^{*} + \tau_{L}\tau_{L}^{*})(\nabla U_{+}^{an}\nabla U_{-}^{nb} + \nabla U_{-}^{an}\nabla U_{+}^{nb}) + \right. \\ + 2\tau_{L}\tau_{R}^{*}\nabla U_{-}^{an}\nabla U_{-}^{nb} + 2\tau_{L}^{*}\tau_{R}\nabla U_{+}^{an}\nabla U_{+}^{nb} \right) + \\ + \frac{\hbar\omega}{E_{nb}^{2} - \hbar^{2}\omega^{2}} (\tau_{R}\tau_{R}^{*} - \tau_{L}\tau_{L}^{*})(\nabla U_{+}^{an}\nabla U_{-}^{nb} - \nabla U_{-}^{an}\nabla U_{+}^{nb}) \right],$$
(3.13)

where $U_{\pm} = \left(\frac{\partial U}{\partial u_x} \pm i \frac{\partial U}{\partial u_y}\right) / \sqrt{2}$. Similar to the case of the optical inverse Faraday effect, only $\tau_R \tau_R^* - \tau_L \tau_L^*$ transforms as a magnetic field, which allows us to drop all other terms and write down:

$$H_{\text{eff}}^{ab} = -\frac{\hbar\omega}{E_{nb}^{2} - \hbar^{2}\omega^{2}} (\tau_{R}\tau_{R}^{*} - \tau_{L}\tau_{L}^{*}) \sum_{n} \left[\left(\nabla U_{+}^{an} \nabla U_{-}^{nb} - \nabla U_{-}^{an} \nabla U_{+}^{nb} \right) \right]. \tag{3.14}$$

For clarity, we can also rewrite Eq. (3.14) in Cartesian coordinates to obtain:

$$H_{\text{eff}}^{ab} = -(\tau \times \tau^*)_z \sum_{n} \frac{\hbar \omega}{E_{nb}^2 - \hbar^2 \omega^2} \left(\langle a | \nabla U | n \rangle \times \langle n | \nabla U | b \rangle \right)_z. \tag{3.15}$$

Here, we point out that the effective Hamiltonian describing the effect of the axial phonons has a form similar to the effective Hamiltonian in Eq. (3.8), which describes the optical inverse Faraday effect. It is composed of two parts: the time-reversal-symmetry-breaking field, expressed as $\tau_R \tau_R^* - \tau_L \tau_L^*$ for phonons and $\mathcal{E}_R \mathcal{E}_R^* - \mathcal{E}_L \mathcal{E}_L^*$ in the optical case, and a contribution arising from the coupling between the perturbation and the electronic states. In the case of phonons, this coupling is described by the action of the operator ∇U on the electronic states. In contrast, for the laser field, the coupling is represented by the action of the r_\pm operator. We can thus conclude that the optical and phonon inverse Faraday effects both arise from a circularly polarized field which acts as a perturbation and couples to the electronic states. In both cases this field leads to time reversal symmetry breaking and hence magnetization. However, the perturbations responsible for these effects arise from different origins, and the nature of the coupling also differs. The similarities and differences between the optical inverse Faraday effect and the phonon inverse Faraday effect are summarized in Table 3.1.

	Phonon IFE	Optical IFE
Perturbation source	Lattice vibrations	Laser field
TRS-breaking field	$ au_R au_R^*- au_L au_L^*$	$\mathscr{E}_R\mathscr{E}_R^*-\mathscr{E}_L\mathscr{E}_L^*$
Perturbation amplitude	$v(t) = \tau_0 \cdot \nabla_{\tau}^2 U$	$v(t) = e\mathbf{r} \cdot \mathscr{E},$

Table 3.1: Comparison between phonon and optical inverse Faraday effects.

To generalize the simple single ion model to describe a crystal lattice, we start by quantizing the phonon modes μ and ν and writing them as:

$$\begin{split} \tau_{p\mu} &= i \sum_{q} e^{iq \cdot R_{p}} l_{q\mu} (\hat{a}_{q\mu} + \hat{a}_{-q\mu}^{\dagger}), \\ \tau_{p\nu} &= \sum_{q} e^{iq \cdot R_{p}} l_{q\nu} (\hat{a}_{q\nu} + \hat{a}_{-q\nu}^{\dagger}). \end{split} \tag{3.16}$$

Here, we introduce bosonic creation and annihilation operators $\hat{a}_{q\mu}^{\dagger}$ and $\hat{a}_{q\mu}^{\dagger}$. The sum $(\hat{a}_{q\mu} + \hat{a}_{-q\mu}^{\dagger})$ now describes the number of phonons contributing to the phonon mode, and the quantity $l_{q\nu} = \sqrt{(\hbar/2\omega_{q\nu})}$ is referred to as the zero-point displacement [20].

In order to describe the coupling between the phonons and the electronic states, we use electron-phonon matrix elements defined as [20]:

$$g_{mn\nu}(\mathbf{k}, \mathbf{q}) = \langle m, \mathbf{k} + \mathbf{q} | \sum_{p} l_{\mathbf{q}\nu} e^{i\mathbf{q} \cdot \mathbf{R}_{p}} \frac{\partial U}{\partial \tau_{p\nu}} | n, \mathbf{k} \rangle.$$
 (3.17)

Electron-phonon matrix elements of this form describe the probability amplitude of an electron in a state $|n, k\rangle$ absorbing a phonon described by a wave vector \mathbf{q} at a frequency mode v and scattering into a new state $|m, k + \mathbf{q}\rangle$. This process is illustrated in the vortex diagram shown in Fig. 3.1. Using Eq. (3.16) and (3.17) in the expression for the effective Hamiltonian given by Eq. (3.15) gives us the effective Hamiltonian:

$$\mathcal{H}_{\text{eff}}^{ab}(\mathbf{k}) = -i\hbar\omega_{\text{ph}} \sum_{\mathbf{q}} \left[(\hat{a}_{-\mathbf{q},\mu}^{\dagger} + \hat{a}_{\mathbf{q},\mu})(\hat{a}_{-\mathbf{q},\nu}^{\dagger} + \hat{a}_{\mathbf{q},\nu}) \right] \times \sum_{\mathbf{q}} \frac{g_{an\mu}(\mathbf{k},\mathbf{q})g_{bn\nu}^{*}(\mathbf{k},\mathbf{q}) - g_{an\nu}(\mathbf{k},\mathbf{q})g_{bn\mu}^{*}(\mathbf{k},\mathbf{q})}{E_{\mathbf{k}nb}^{2} - \hbar^{2}\omega_{\text{ph}}^{2}} \right]. \quad (3.18)$$

This effective Hamiltonian describes the effect of axial phonons on the electronic levels in a crystal. Similarly to Eq. (3.15), it shows a dependence on the displacement in the form of $(\hat{a}_{-q,\nu}^{\dagger} + \hat{a}_{q,\nu})$ and $(\hat{a}_{-q,\mu}^{\dagger} + \hat{a}_{q,\mu})$ operators. The coupling of the displacement to the electronic energy levels is represented by the electron-phonon matrix elements. Importantly, Eq. (3.18) is material independent and provides a way of estimating the size of the effect, which we discuss in the next section.

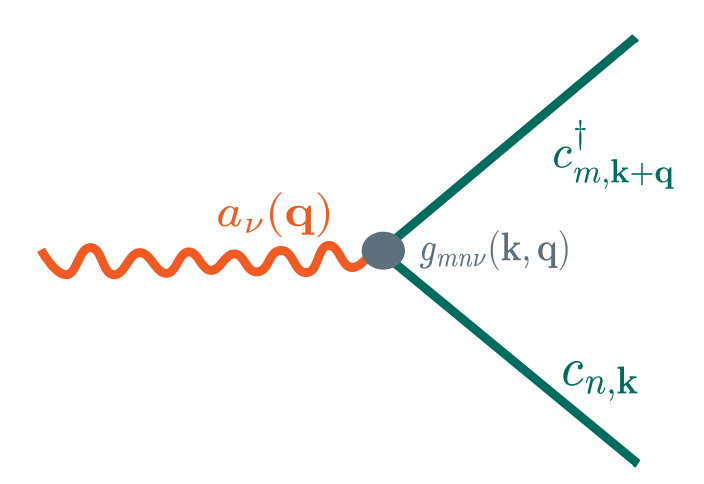


Figure 3.1: Vortex diagram illustrating an electron scattering from state $|n, k\rangle$, labeled by annihilation operator $c_{n,k}$, to state $|m, k+q\rangle$, labeled by creation operator $c_{m,k+q}^{\dagger}$, after absorbing a phonon of mode v and wave vector \mathbf{q} , denoted by phonon annihilation operator $a_v(\mathbf{q})$. The probability amplitude of this process is given by the electron-phonon matrix elements $g_{mnv}(\mathbf{k},\mathbf{q})$

3.3 Effective magnetic field in SrTiO₃

To evaluate how well Eq. (3.18) describes the phonon-induced magnetization, we use it to predict the effective magnetic field arising from axial phonons in a sample of SrTiO₃. In our choice of material we are motivated by the recent experimental observations of the large magnetic moment in SrTiO₃ [16]. In the experiment involving the magneto-optical Kerr effect described in Chapter 2, a circularly polarized laser pulse was used to drive the soft phonon mode at the Γ point, i.e., the phonon mode at q=0. To simplify the further calculations, we rewrite the operators $\hat{a}_{q\nu}$ and $\hat{a}_{q\mu}$, in vector form, i.e., we define \hat{a}_q and \hat{a}_{-q}^{\dagger} , such that $\varepsilon \hat{a}_q = \begin{pmatrix} \hat{a}_{q,\nu} \\ \hat{a}_{q,\nu} \end{pmatrix}$ and $\varepsilon^* \hat{a}_{-q}^{\dagger} = \begin{pmatrix} \hat{a}_{-q,\nu}^{\dagger} \\ \hat{a}_{-q,\nu}^{\dagger} \end{pmatrix}$. This allows us to rewrite Eq. (3.18) as

$$H_{\text{eff}}^{ab}(\mathbf{k}) = -2i\hbar\omega_{\text{ph}} \sum_{\mathbf{q}} \left[\left(\hat{a}_{-\mathbf{q}}^{\dagger} \hat{a}_{\mathbf{q}} + \frac{1}{2} \delta_{-\mathbf{q}, \mathbf{q}} \right) \right.$$

$$\times \sum_{n} \frac{g_{an\mu}(\mathbf{k}, \mathbf{q}) g_{bn\nu}^{*}(\mathbf{k}, \mathbf{q}) - g_{an\nu}(\mathbf{k}, \mathbf{q}) g_{bn\mu}^{*}(\mathbf{k}, \mathbf{q})}{E_{\mathbf{k}nb}^{2} - \hbar^{2} \omega_{\text{ph}}^{2}} \right]. \tag{3.19}$$

Here, we have used the bosonic anticommutation relations and the orthonormality property of the polarization vectors from Eq. (2.7). Further, we have assumed that the degenerate modes contribute equally to the circularly polarized mode, i.e., $\varepsilon_{\mu}=\varepsilon_{\nu}$, and, following Ref. [38], omitted the terms containing $\hat{a}_{q}\hat{a}_{q}$ and $\hat{a}_{-q}^{\dagger}\hat{a}_{-q}^{\dagger}$. With this

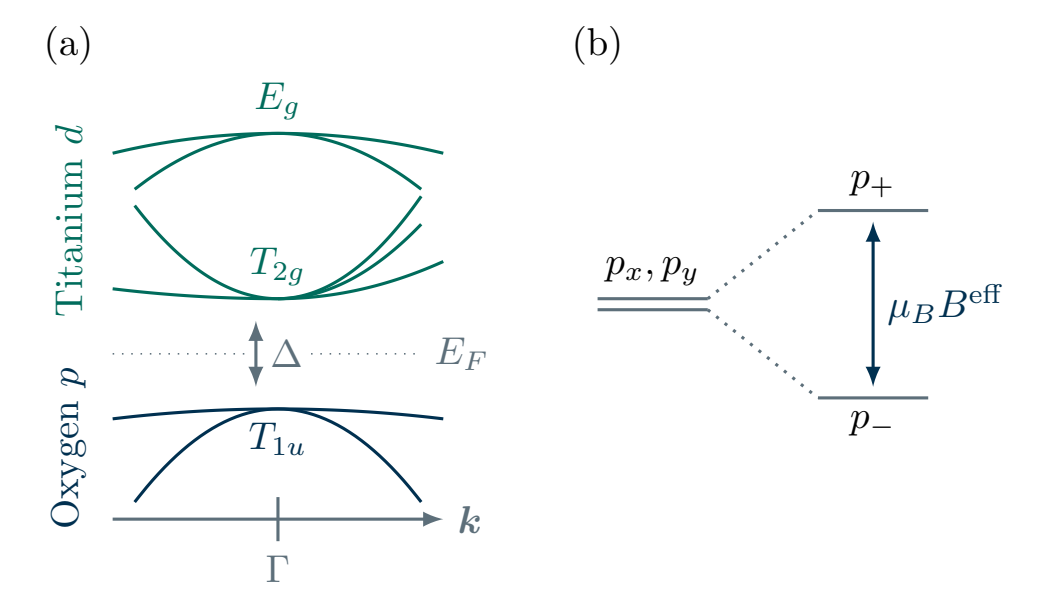


Figure 3.2: Illustration of the electronic structure of $SrTiO_3$. a) Valence bands composed of oxygen p-states and conduction bands consisting of Ti d-states. b) Splitting of p-bands under the influence of the effective magnetic field by analogy with the Zeeman effect.

expression, evaluating only the phonons at the Γ -point, leaves us with the effective Hamiltonian expressed in terms of the phonon number operator \hat{n}_0 :

$$H_{\text{eff}}^{ab}(\mathbf{k}) = -2i\hbar\omega_{\text{ph}} \left[\left(\hat{n}_0 + \frac{1}{2} \right) \right.$$

$$\times \sum_{n} \frac{g_{an\mu}(\mathbf{k}, 0)g_{bn\nu}^*(\mathbf{k}, 0) - g_{an\nu}(\mathbf{k}, 0)g_{bn\mu}^*(\mathbf{k}, 0)}{E_{\mathbf{k}nb}^2 - \hbar^2\omega_{\text{ph}}^2} \right]. \tag{3.20}$$

To approximate the size of the effective magnetic field, we study the electronic structure of SrTiO₃. Oxygen *p*-states constitute the valence band, while Ti-*d* states compose the conductance band, as shown in Fig. 3.2. We expect the magnetic field to induce a splitting of *p*-states in analogy with the Zeeman splitting [39]. We thus expect the *p*-states to take the form $p_{\pm} = \frac{1}{\sqrt{2}}(p_x \pm ip_y)$. Therefore, we calculate the overlap elements $H_{\text{eff}}^{xy}(0)$ and $H_{\text{eff}}^{yx}(0)$, where we set k=0 because we are interested in electrons at the Γ point. In order to do this, we first observe that the phonon mode and electron *p*-states are parity odd. Therefore, the electron in the *p*-state absorbing a phonon can only scatter to the parity-even state, i.e., Ti-*d* states. Moreover, since SrTiO₃ has a large band gap of $\Delta = 3.75$ eV for the direct band gap [40], and H_{eff} decreases quadratically with the size of the gap, we assume that we only need to consider the overlap elements

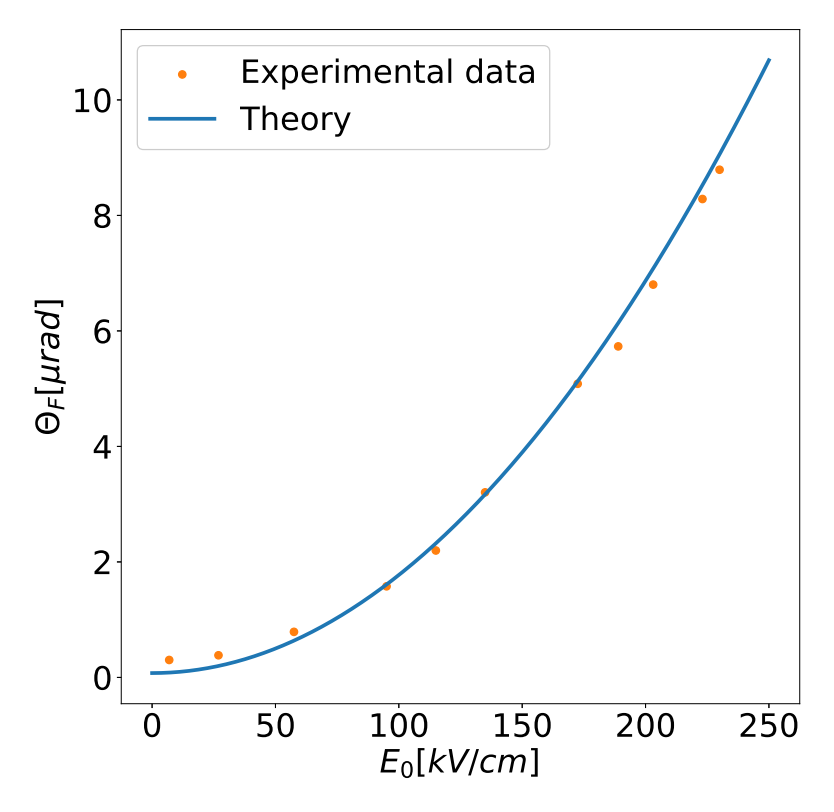


Figure 3.3: Polarization rotation as a function of electric field strength of the pump laser, calculated with |g| = 7 meV. The solid line represents the values obtained using Eq. (3.25), while the dots represent the experimental data from Ref. [16].

corresponding to the gap. Thus, we get the final expression:

$$H_{\text{eff}}^{xy}(\mathbf{k} = 0) = -H_{\text{eff}}^{yx}(\mathbf{k} = 0) = -i\left(\hat{n}_0 + \frac{1}{2}\right) \frac{\hbar\omega_{\text{ph}} |g|^2}{\Delta^2 - \hbar^2\omega_{\text{ph}}^2}.$$
 (3.21)

Here, g is the electron-phonon coupling strength determined by the electron-phonon matrix elements [41]. To calculate the energy level splitting, it is useful to switch basis to p_{\pm} as opposed to p_x , p_y . The Hamiltonian in this basis can be expressed as $H_{\rm eff}^{\pm\pm}=\pm iH_{\rm eff}^{xy}$. Thus, we can deduce the energy levels:

$$E^{\pm} = \pm \frac{\hbar \omega_{\rm ph} |g|^2}{\Delta^2 - \hbar^2 \omega_{\rm ph}^2} \left(\hat{n}_0 + \frac{1}{2} \right).$$
 (3.22)

With the size of the splitting of the electronic energy levels $\Delta E = E^+ - E^-$, we can calculate the effective magnetic field by comparing ΔE to the splitting expected for the

Zeeman effect, i.e., $\frac{\Delta E_{\text{Zeeman}}}{2} = g_z \mu_B B_z^{\text{eff}}$. Therefore, the effective magnetic field can be calculated using the following equation:

$$\frac{\hbar\omega_{\rm ph}|g|^2}{\Delta^2 - \hbar^2\omega_{\rm ph}^2} \left(\hat{n}_0 + \frac{1}{2}\right) = g_J \mu_B B_z^{\rm eff}.$$
 (3.23)

The soft mode in SrTiO₃ has a frequency of $\omega_{\rm ph}=2\pi\times2.7$ THz [16], and we assume $g_J=1$. Therefore, in order to provide an estimate for $B_z^{\rm eff}$ we need to approximate the phonon number \hat{n}_0 . In the SrTiO₃ experiment [16], a circularly polarized laser with a laser field strength of $E_0=230$ kV/cm was used. Additionally, a screening constant of $\beta=0.7$ was applied to reflect the fact that not all of the incoming field strength will be absorbed into the sample and give rise to axial phonons. Thus, we calculate the peak intensity of the laser as:

$$I_{\text{max}} = \frac{1}{2\mu_0 c} \widetilde{E}_0^2, \tag{3.24}$$

where $\widetilde{E}_0 = \beta E_0$. Here, we make the assumption that at the resonant frequency, i.e., $\omega = \omega_{\rm ph}$, one photon from the laser pulse will excite one axial photon. Thus, with the energy of a single photon $\hbar \omega$ we can approximate the number of incident photons per unit cell as n=30 1/ps. Here we have used the fact that the intensity is defined as the amount of incident energy per time per area. The area of the unit cell of SrTiO₃ was calculated as $A=a^2$, where the lattice constant is a=3.9 Å. Given the pulse length of 2 ps in agreement with Ref. [16], we set the total number of phonons as $N_{\rm ph}=N=60$. Thus, the electron-phonon coupling strength remains the only free parameter in Eq. (3.23). Setting it to g=7 meV [41, 42] renders $B^{\rm eff}\approx 40$ mT, in line with 32 mT observed in the experiment [16].

Eq. (3.23) also allows us to calculate the angle of the Faraday rotation, which is a rotation of polarization that a linearly polarized pulse acquires after passing through a magnetized material. Faraday rotation and Kerr rotation are closely related, and differ by no more than factor of 2 [16]. Therefore calculating the Faraday rotation allows us to compare our findings with the experimental observations. Thus, we calculate the Faraday rotation θ_F as follows [16, 26]:

$$\theta_F = \frac{l_{\text{decay}}V}{2}B_z^{\text{eff}}$$

$$= \frac{l_{\text{decay}}V}{2}\frac{1}{\mu_B}\frac{\hbar\omega|g|^2}{\Delta^2 - \hbar^2\omega^2}\left(n_0 + \frac{1}{2}\right).$$
(3.25)

Here, V is the Verdet constant, which for SrTiO₃ is given by $V \approx 180 \text{ rad m}^{-1}\text{T}^{-1}$ and $l_{\text{decay}} = 2.5 \ \mu\text{m}$ is the penetration depth [16]. Eq. (3.25) allows us to plot the Faraday rotation as a function of the electric field strength of the circularly polarized pump field.

Plotting the experimental data [16] on the same axis shows that the microscopic theory presented above achieves a good agreement with the experiment. The plot with this comparison is presented in Fig. 3.3.

Here, it is important to note that our calculation above was based on the simple assumption that one photon of the pump laser excites one circularly polarized phonon, which led us to the phonon number N=60. This number is related to the phonon displacement through [25]

$$N = \frac{\omega_{\rm ph}}{\hbar} u^2. \tag{3.26}$$

At the same time, we can classically calculate the phonon normal mode displacement expected from a laser field by solving the classical equation of motion, Eq. (4.7), as explained in more detail in Chapter 4. From Eq. (3.26) and Eq. (4.7) we can calculate that the laser field strength corresponding to $E_0 = 230$ kV/cm should result in the number of phonons on the order of $N \approx 0.24$. Similarly, Caruso *et al.* estimate that the number of phonons arising from a THz pulse should be on the order of $N \approx 1$ [43].

However, this estimate originates from the assumption that the pump laser field excites, i.e., creates new vibrations in the material. This, however, does not address the role of thermal vibrations that are already present in the sample. At room temperature T = 300 K, we can expect around two phonons. This can be calculated using the Bose-Einstein distribution [39]:

$$N_{\rm ph}^{\rm BE} = \frac{1}{\exp\left(\frac{\hbar\omega_{\rm ph}}{k_BT}\right) - 1}.$$
 (3.27)

If the incoming circularly polarized laser polarizes the existing phonons rather than exciting new ones, then the expected phonon number needs to be calculated differently than the described estimation for SrTiO₃.

In addition, the accuracy of the estimate of the effective magnetic field depends to a greater extent on the accuracy of the electron-phonon coupling strength. At the same time, obtaining a good estimate of the electron-phonon matrix elements at the Γ -point in $\mathrm{SrTiO_3}$ presents a challenge. Recent calculations show that the electron-phonon coupling strength can vary greatly around the Γ -point in $\mathrm{SrTiO_3}$ [41]. Although for the ferroelectric soft mode investigated here, it remains of the order of 1-10 meV, it can increase dramatically when the phonon k-vector is no longer precisely zero. At the same time, Eq. (3.23) shows that the effective magnetic field B_z^{eff} depends quadratically on |g|. Therefore, a variation in the electron-phonon coupling strength greatly affects the results, which makes a precise calculation of |g| at the Γ point crucial for obtaining an accurate estimate of the magnetic field.

Moreover, when deriving our main result given by Eq. (3.18), we have assumed that $\nabla_{\tau}U$ is real, i.e., $\nabla_{\tau}U = (\nabla_{\tau}U)^*$. Typically, it is a reasonable assumption, since as long as $\nabla_{\tau}U$ is Hermitian, it can always be transformed into a basis where it would also be

real. However, since we have allowed τ to be complex, a more general starting point would be to assume that $\nabla_{\tau}U$ is also complex. Therefore, there could be an additional contribution to the effective Hamiltonian in Eq. (3.18) arising from the complex part of $\nabla_{\tau}U$ operator. Investigating this contribution is one of the directions of our future research.

Therefore, while the results presented in Fig. 3.3 present the same quadratic dependency on the electric field strength as was observed in the experiment [16], a more accurate approximation of the phonon number and electron-phonon coupling strength is needed to provide a better estimate of the expected effective magnetic field. Additionally, one needs to take into account potential contributions from the complex part of the $\nabla_{\tau} U$ operator.

We have thus presented a microscopic theory that explains the magnetization arising from axial phonons by considering electron-phonon coupling as the perturbation to the full Hamiltonian of the crystal. However, this formalism does not explore the nature of the effective magnetic field, since it is approximated through the size of the splitting of the electronic levels. In theory, such splitting could be caused by a time-reversal symmetry breaking field that is not necessarily a magnetic field. In the next chapter, we discuss possible ways to investigate this topic.

Axial phonons and (anomalous) Hall effect

In this chapter we describe how the conventional and anomalous Hall effect can be used to improve our understanding of phonon-magnetic effects. Specifically, we explore the possibility of using these effects to answer the question of whether the effective magnetic field arising from the axial phonons is a real magnetic field obeying Maxwell's equations, or an effective magnetic field that merely imitates its effects, such as time reversal symmetry breaking. This directly relates to the second research question mentioned in Chapter 1, as it concerns a property of the phonon-induced magnetic field that remains unresolved. We first present this problem in section 4.1. Then we give a brief introduction to the Hall effect and the anomalous Hall effect in section 4.2, followed by a description of a proposed experimental setup in section 4.3. Finally, in section 4.4 we present a way to calculate the expected size of the conventional Hall effect.

4.1 Real vs effective magnetic field

To present the open question of the nature of the phonon-induced magnetic field, we return to the experiments of the phonon magnetic moment described in Chapter 2. It is worth noting that these experiments observe the magnetization 'by proxy', i.e., by measuring an observable that is closely related to the magnetization. Thus, in phonon Zeeman effect experiments the phonon magnetic moment is calculated from the observed size of the splitting of phonon frequencies [3–15] by applying Eq. (2.16). Similarly, the experiments utilizing magneto-optical effects measure the angle of the polarization rotation as the probe field is reflected from the material. The emerging magnetic field can be calculated from the angle of the polarization rotation, [16, 17] as described in

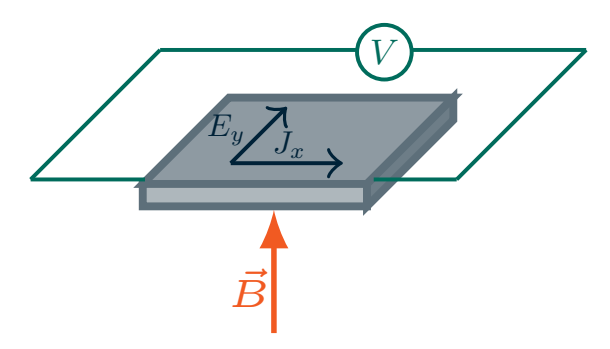


Figure 4.1: Illustration of the Hall effect. Voltage V passes current J_x through the material. The magnetic field B, perpendicular to the plane of the current, induces a transverse electric field E_y that is perpendicular to both the current and the magnetic field.

more detail in Chapter 3. Neither of the methods measures the magnetic field directly, which poses the question if the magnetic field is a real, Maxwellian magnetic field or an *effective* magnetic field which sometimes causes the same phenomena (e.g., splitting of phonon frequencies or rotation of polarization of the probe field) as a Maxwellian magnetic field would, while being a different physical quantity.

In light of this question, an alternative explanation for the results of the pump-probe experiments was proposed. It has been suggested that the large rotation of polarization observed by, e.g., Basini et al. [16] is caused by the coupling of the time reversal symmetry breaking pump field to the linearly polarized probe field inside the material and thus causing the rotation of polarization [44, 45]. As a result, there is no emergent magnetic field, but only the imitation of its effects by the circularly polarized pump field. Therefore, this effective field would not be measurable outside of the material.

However, the experiment involving a switching of magnetic order in a layer placed on top of the layer excited with a circularly polarized pump field [18] contradicts this idea since in this case axial phonons seem to have a direct effect on the layer of material placed outside of the sample excited by the pump laser.

Thus, the nature of the phonon-induced effective magnetic field remains an open question. Therefore, we suggest a method for investigating whether this magnetic field is a real magnetic field or merely an effective field, based on the conventional and anomalous Hall effects.

4.2 Hall effect and Anomalous Hall effect

Here, we give a brief introduction of the Hall effect and the anomalous Hall effect. While they are both characterized by the presence of transverse conductivity and can be observed in, e.g., graphene, there are some substantial differences between them which are relevant for studying phono-magnetic effects.

The Hall effect can be observed in a layer of material subjected to a voltage that passes a current J through the material. When a perpendicular magnetic field is applied to such a system, the electrons flowing through the layer of the material start to experience the Lorentz force [46]:

$$F = e(E + v \times B). \tag{4.1}$$

Here, v is the velocity of the electrons proportional to the current J and B is the applied magnetic field. According to the equation above, in a steady state, where F = 0, a transverse electric field E has to be present, perpendicular to the applied magnetic field and the current. Conductivity σ and resistivity ρ are thus defined as tensors [1]:

$$J_{\mu} = \sigma_{\mu\nu} E_{\nu}$$

$$E_{\mu} = \rho_{\mu\nu} J_{\nu}.$$
(4.2)

In 2D materials, such as graphene, the Hall effect can become quantized, transforming into the quantum Hall effect. This is typically achieved at low temperatures and strong magnetic fields of the order of 10 T [47]. This effect is a consequence of Landau levels, i.e., energy levels for free non-relativistic particles in the presence of an external magnetic field: [1]

$$E_n = \hbar \omega_e \left(n + \frac{1}{2} \right). \tag{4.3}$$

In the equation above $\omega_e = \frac{eB}{cm}$ is referred to as the cyclotron frequency, where B is the applied magnetic field. Here, n is a quantum number that can only assume integer values. It can be shown that the number of filled Landau levels is given by [48]

$$N = \text{floor}\left(\frac{2\pi\hbar c}{gqB}\delta N\right),\tag{4.4}$$

where δN is the charge carrier density and g is the Dirac cone degeneracy. The function 'floor' comes from the fact that N is an integer number. In graphene, the transverse conductivity, σ_{xy} and resistivity ρ_{xy} are related to the number of filled Landau levels through:

$$\sigma_{xy} = \frac{4e^2}{h} \left(N + \frac{1}{2} \right),$$

$$\rho_{xy} = \frac{1}{\sigma_{xy}} = \frac{h}{4e^2} \frac{1}{N + \frac{1}{2}}.$$
(4.5)

For small magnetic fields, the resistivity increases linearly with the magnetic field, but in the strong magnetic field regime, it becomes quantized.

Given the experimental observations for $SrTiO_3$ [16], the magnetic field arising from axial phonons is not enough to enter the quantum Hall regime. However, the conventional Hall effect is possible.

The theory for the anomalous Hall effect was first proposed by Haldane, who considered a honeycomb lattice similar to graphene with no external magnetic field [49] and showed that quantum Hall effect can be achieved without an external magnetic field, as long as the system breaks time-reversal symmetry. This can be achieved through spin-orbit coupling or if the material itself is intrinsically magnetic. Qiao *et al.* propose a method of realizing the anomalous Hall effect in graphene, which is inherently challenging since graphene does not exhibit a significant spin-orbit coupling and is also non-magnetic [50, 51]. This method consists of placing graphene on top of a substrate, which leads to the emergence of the exchange coupling between the graphene layer and the substrate. Additionally, graphene acquires Rashba spin-orbit coupling (SOC) [52], and the graphene Hamiltonian takes the following form:

$$H = -t \sum_{\langle ij \rangle \alpha} c^{\dagger}_{i\alpha} c_{j\alpha} + i t_{SO} \sum_{\langle ij \rangle \alpha\beta} \hat{e}_z \cdot \left(\boldsymbol{\sigma} \times \boldsymbol{d}_{ij} \right) c^{\dagger}_{i\alpha} c_{j\beta} + \lambda \sum_{i\alpha} c^{\dagger}_{i\alpha} \sigma_z c_{i\alpha}. \tag{4.6}$$

Here, the first term corresponds to the pristine graphene Hamiltonian with hopping constant t, and the second term comes from the Rashba SOC with $t_{\rm SO}$ being the strength of the Rashba SOC coupling and σ the Pauli vector. The third term is caused by the exchange field with λ denoting its strength.

For such a setup, the material chosen as the substrate needs to be an antiferromagnetic insulator. The insulating quality ensures that the graphene is the only transport channel, which affects the exchange term in Eq. (4.6). The antiferromagnetic properties are necessary because a ferromagnet would apply a magnetic field to the graphene layer, which would complicate the detection of the anomalous Hall effect.

4.3 The setup

In this section, we propose an experimental setup that would utilize the conventional and the anomalous Hall effects to determine the nature of the phonon-induced magnetic field. The setup is depicted in Fig. 4.2 and consists of a sample of a layer of graphene placed on top of a sample of SrTiO₃. The SrTiO₃ sample is then subjected to a circularly polarized laser pulse which causes the appearance of axial phonons and hence the magnetization of the material. The magnetic field is then measured in the graphene layer, as well as the transverse conductivity characteristic of the conventional and the anomalous Hall effect.

This double measurement setup allows to understand the nature of the phonon-induced magnetization in the following way: If the external magnetic field in the graphene layer is non-zero after driving the axial phonons with the pump field, it shows that the circularly polarized phonons give rise to a real, Maxwellian magnetic field. On the other hand, if the magnetic field in the graphene is measured to be zero, but simultaneously there is a non-zero transverse resistivity, it shows that axial phonons



Figure 4.2: The experimental setup consisting of a sample of $SrTiO_3$ and a layer of graphene placed on top of it. A circularly polarized laser pulse is applied to the $SrTiO_3$ sample. Thus, a magnetic field \mathbf{B} is expected to emerge due to the axial phonons driven by the laser pulse.

give rise to a field that mimics the effect of a magnetic field through time-reversal symmetry breaking, as expected in the anomalous Hall effect. Measuring the transverse resistivity therefore acts as a way to verify that axial phonons are present in the material after the sample has been driven by a circularly polarized pump laser field. The setup proposed above should be possible to perform given the right equipment. As a complement to the experimental measurement, an estimate of the expected values of transverse resistivity and magnetic fields needs to be provided, in order to compare the observations with the theoretical predictions. In the next section we propose a way to make such an estimate.

4.4 Magnetic field and transverse resistivity calculation

To calculate the size of the magnetic field and transverse resistivity that can be measured in the setup described in section 4.3, we first have to calculate the displacement and the phonon angular momentum arising from the laser pump. To do that, we turn to the classical equation of motion:

$$\ddot{\boldsymbol{u}} + \eta \dot{\boldsymbol{u}} + \omega_{\rm ph}^2 \boldsymbol{u} = Z \boldsymbol{E} e^{i\omega t}. \tag{4.7}$$

Here, η is the damping parameter, ω is the frequency of the circularly polarized laser, E is the laser field strength and Z is the effective charge. For SrTiO₃, the parameters of this equation are known: the damping parameter is given by $\eta = 2\pi \times 0.63$ THz and

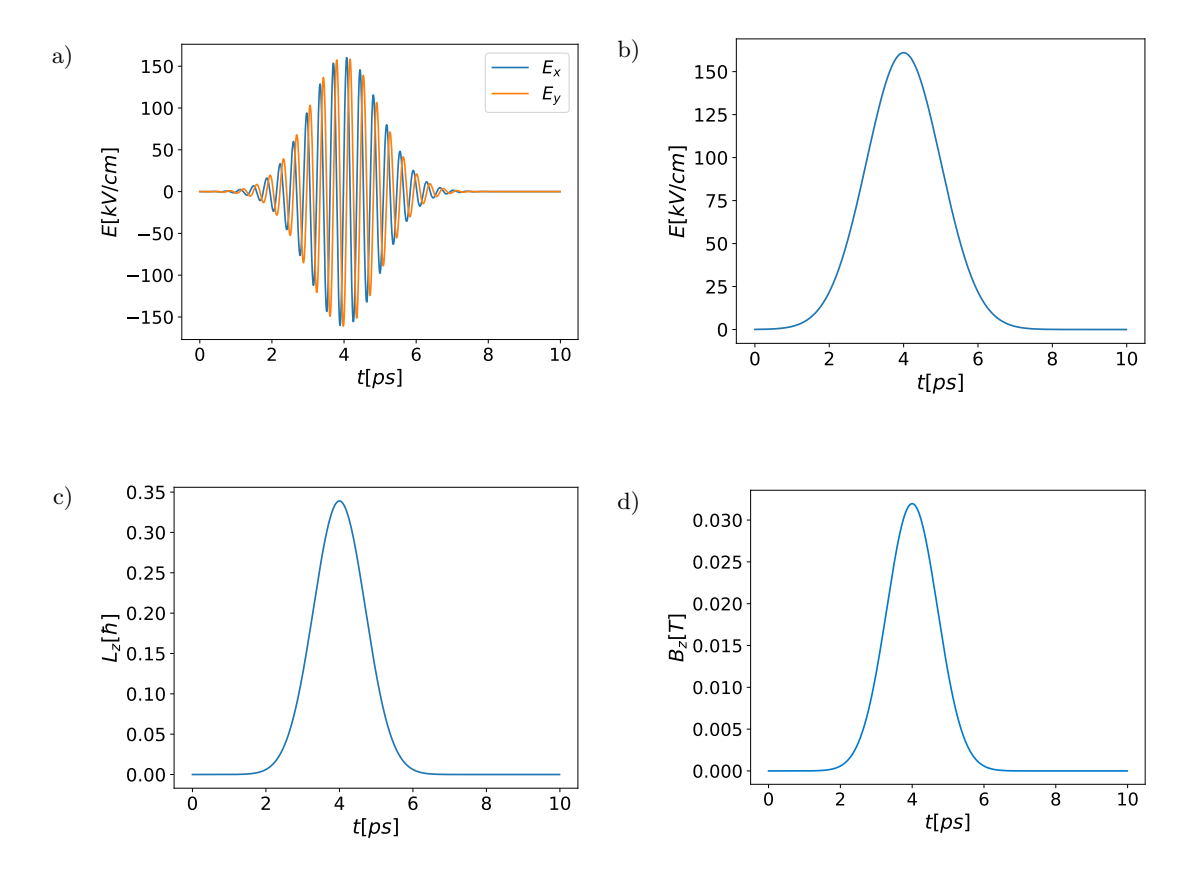


Figure 4.3: a) x- and y-components of the electric field strength E modeled to correspond to the pump laser field strength used by Basini et al. [16]. b) The corresponding amplitude of the electric field strength. c) The resulting phonon angular momentum calculated using the classical equation of motion. d) Magnetic field strength calculated by determining the gyromagnetic constant γ and distance to the dipole r_z phenomenologically.

the phonon frequency at the Γ -point is $\omega_{\rm ph}=2\pi\times2.7$ THz at 300K [53]. The effective charge is given by 1.54 e Da $^{-\frac{1}{2}}$ [16]. In order to achieve the driving of the phonons by the circularly polarized pump field, we set the laser frequency to be in resonance with the phonon frequency, i.e., $\omega=2\pi\times2.7$ THz. The phonon angular momentum is then obtained by solving Eq. (4.7) analytically:

$$L_z = u_x \dot{u}_y - \dot{u}_x u_y = \frac{Z^2 E^2 \omega}{(\omega_{\rm ph}^2 - \omega^2)^2 + \eta^2 \omega^2}.$$
 (4.8)

Here, the electric field is directed along the *z*-axis. In order to calculate the magnetic field, we approximate it as a magnetic field due to a magnetic dipole:

$$B_z = \frac{\mu_0 m_z}{2\pi r_z^3} = \frac{\mu_0 \gamma L_z}{2\pi r_z^3}.$$
 (4.9)

Then, the transverse resistivity can be calculated using Eq. (4.5). However, before we can perform this calculation, we need to set the material specific parameters from Eq. (4.9), namely, the gyromagnetic constant, γ and the distance between the graphene layer and the magnetic dipole, r_z^3 . In order to do that, we use the values recorded in the recent pump-probe experiment on SrTiO₃ involving the magneto-optical Kerr effect [16], which is described in more detail in Chapter 2. We first model the electric field strength to correspond to the pump-field used in the experiment using a Gaussian embedding:

$$E(t) = \beta E_0 e^{-\frac{(t-t_0)^2}{2\sigma^2}}. (4.10)$$

Here, $\beta=0.7$ is the screening constant. Furthermore, we set the maximum electric field strength to $E_0=230$ kV/cm, the pulse peak to $t_0=4$ ps and $\sigma=1$ ps in order to be consistent with Ref. [16]. With these parameters and Eq. (4.8) we can calculate the angular momentum resulting from axial phonons driven by the pump laser with the laser field strength given by Eq. (4.10)

Now, we can phenomenologically determine the gyromagnetic ratio by using the peak value of the obtained angular momentum and the experimentally recorded phonon magnetic moment of $\mu_{\rm ph}=0.1\mu_{\rm B}$ [16]. With these values and Eq. (2.15) we determine the gyromagnetic ratio to be $\gamma\approx 268.86$ e/Da

We determine the distance r_z in Eq. (4.9) in a similar way. To detect the experimentally observed value of B=32 mT, the magnetic field has to be measured at a distance of $r_z\approx 1.8$ Å from the Ti-atoms in the SrTiO $_3$ sample, which exhibit a soft phonon mode of the needed frequency. The plots of the electric field strength, its amplitude, as well as the resulting phonon angular momentum and magnetic field strength are shown in Fig. 4.3.

The calculation proposed above makes it possible to provide a similar estimate for a laser of a different strength. Therefore, it can be adapted for a potential future experimental setup.

Summary of papers

Paper I

Phonon Inverse Faraday Effect from Electron-Phonon Coupling

We present a microscopic theory of the magnetization induced by axial phonons based on the formalism of the optical inverse Faraday effect. We consider circularly polarized phonons as a time-dependent perturbation to investigate their effects on electronic energy levels. Using second-order perturbation theory, we arrive at a general expression for the effective Hamiltonian which describes these effects. In an attempt to validate our findings by comparing with experimental observation, we apply the resulting equation to the case of $SrTiO_3$ sample driven with a circularly polarized laser field. We calculate the size of the splitting of electronic energy levels in $SrTiO_3$ which allows us to estimate the size of the emergent magnetic field and reach a good agreement with the experiment.

Paper II

Axial phono-magnetic effects

In this review paper we summarize and present recent advances in understanding the phono-magnetic effects. We first phenomenologically motivate the connection between phonon angular momentum and the arising magnetization. Further, we present the experimental observations that confirm that axial phonons influence the magnetic properties of the material, giving rise to a magnetic moment that has been measured to be larger than can be expected from the ionic mass. Finally, we give an overview of recently proposed theories that strive to explain this effect. We conclude by discussing the similarities and connection between the different theoretical approaches.

Conclusion and outlook

6.1 Conclusion

To conclude this thesis, we revisit the research questions posed in Chapter 1, the first of which asks:

Apart from ionic motion, what other effects can influence phono-magnetic effects resulting in the large magnetization observed experimentally?

As explored in Chapter 2, the experimental observations conflict with the classical explanation of phono-magnetic effects based on the ionic motion. At the same time, the gyromagnetic ratios of electrons and ions suggest that electrons play a part in the emergence of this effect. Furthermore, several recently proposed microscopic theories striving to explain the phonon-induced magnetization involve examining the interplay between axial phonons and electrons. However, while the theories seem to agree on the importance of electron-phonon interaction, the explanations of how exactly this interaction becomes relevant vary.

In Chapter 3 we have summarized a theory explaining phonon-induced magnetization by considering the circularly polarized phonons as a second-order perturbation, which couples to the electronic states through electron-phonon coupling. This allows us to view phonon-induced magnetization as a vibrational analogue to the optical inverse Faraday effect. Our framework of the phonon inverse Faraday effect leads to good agreement with the experimental observations. Therefore, it solidifies the proposition that large phonon-induced magnetization originates from the electron-phonon coupling.

In addition to the challenge of finding a microscopic theory accurately predicting the size of the magnetization arising from axial phonons, the nature of the induced magnetic field remains not entirely understood. This issue was reflected in our second question:

How can we better understand the nature of the magnetization induced by axial phonons and how does it affect other physical phenomena such as the Hall effect?

Chapter 4 presents our approach to this question through the use of the conventional and anomalous Hall effects. We have outlined the way these effects could be utilized in an experiment that would determine whether the magnetic field induced by axial phonons is a Maxwellian field or merely an effective field that only breaks time-reversal symmetry.

6.2 Outlook

This thesis outlines the progress made towards understanding the phono-magnetic effects. However, our work also points us towards several challenges that remain unsolved.

For example, while we have proposed a microscopic theory explaining phonon-induced magnetism in terms of the phonon inverse Faraday effect, a more exact calculation of the electron-phonon coupling strength is needed to make a more accurate comparison with the experimental observations. Additionally, it would be beneficial to understand the exact role of the drive of the pump laser pulse. Specifically, if the pump laser field excites new vibrational modes that display the same polarization as the laser, or if it polarizes the thermal vibrations that are already present in the material. Moreover, the formalism could be improved by accounting for the contributions of the complex part of the gradient of the potential energy operator.

In addition, since the nature of the magnetic field induced by phonons remains not completely understood, a promising path would be to study the effect of axial phonons on other physical phenomena. We discussed the potential of using the conventional and anomalous Hall effects to understand if the arising field is a Maxwellian field. However, several other phenomena where axial phonons could have a substantial impact remain unexplored.

One such phenomenon is the temperature dependence of the electrical conductivity in strongly correlated systems. These systems are often described by a Hubbard model which accounts for tunneling between electronic sites and the repulsion forces between the electrons of different spins occupying the same site [54]. This model could be modified to account for the influence of the axial phonons by introducing an additional term that includes the interaction between electron spin and phonon angular momentum. We suggest that this coupling will cause spin splitting, the size of which will be determined by the size of the phonon angular momentum. In turn, the phonon

angular momentum induced by thermal vibrations is dependent on the temperature. As the splitting of the bands could potentially influence the conductance if the new bands cross the Fermi level [55], this opens for a potential to influence the temperature dependence of conductivity through axial phonons.

Another largely unexplored area of research on phono-magnetic effects are axial phonons in optical cavities. While optical cavities have been proposed as a way to tune the phonon frequencies [56], the question of how an interaction with an optical cavity may influence the induced effective magnetic field remains open. One way to explore this would be to utilize the effective Hamiltonian discussed in Chapter 3 with corrections for the coupling between the cavity and the phonons.

In summary, while some progress towards understanding and utilizing phono-magnetic effects has already been made, there are still plenty of unanswered questions. For example, it remains to be seen if the large magnetization induced by axial phonons originates from a Maxwellian magnetic field. Additionally, the influence of axial phonons on electric properties remains a promising but largely unexplored area of research. Investigation of these questions promises to be a part of reaching a more complete understanding of phono-magnetic effects.

Acknowledgments

First of all, I would like to thank my supervisor, Matthias, for guidance, encouragement, and inspiring discussions. I am deeply grateful for the opportunity to work with you and to learn from you.

I would also like to thank my examiner, Paul, and my co-supervisor, Julia, for their valuable feedback and support.

I am also very grateful to all my colleagues in the condensed matter and materials theory division for making the office a warm and friendly place.

Last but not least, I would like to thank my family and friends for their encouragement and their willingness to listen to me talk about physics, even when it was probably incomprehensible. Your patience and belief in me have meant more than I can say.

Bibliography

- [1] S. M. Girvin and K. Yang, *Modern condensed matter physics* (Cambridge University Press, 2019).
- [2] C. Kittel, On the Gyromagnetic Ratio and Spectroscopic Splitting Factor of Ferromagnetic Substances, Phys. Rev. 76, 743 (1949). doi:10.1103/PhysRev.76.743.
- [3] G. Schaack, *Magnetic-field dependent phonon states in paramagnetic CeF*₃, Solid State Communications 17, 505 (1975). doi:10.1016/0038-1098(75)90488-3.
- [4] G. Schaack, Magnetic field dependent splitting of doubly degenerate phonon states in anhydrous cerium-trichloride, Zeitschrift für Physik B Condensed Matter and Quanta 26, 49 (1977). doi:10.1007/BF01313371.
- [5] G. Schaack, Observation of circularly polarized phonon states in an external magnetic field, Journal of Physics C: Solid State Physics 9, L297 (1976). doi:10.1088/0022-3719/9/ 11/009.
- [6] B. Cheng, T. Schumann, Y. Wang, X. Zhang, D. Barbalas, S. Stemmer, and N. Armitage, *A large effective phonon magnetic moment in a Dirac semimetal*, Nano letters **20**, 5991 (2020). doi:10.1021/acs.nanolett.0c01983.
- [7] A. Baydin, F. G. Hernandez, M. Rodriguez-Vega, A. K. Okazaki, F. Tay, I. G Timothy Noe, I. Katayama, J. Takeda, H. Nojiri, P. H. Rappl, et al., Magnetic control of soft chiral phonons in PbTe, Physical Review Letters 128, 075901 (2022). doi:10.1103/PhysRevLett.128. 075901.
- [8] C. Tang, G. Ye, C. Nnokwe, M. Fang, L. Xiang, M. Mahjouri-Samani, D. Smirnov, E.-H. Yang, T. Wang, L. Zhang, et al., Exciton-activated effective phonon magnetic moment in monolayer MoS₂, Physical Review B 109, 155426 (2024). doi:10.1103/PhysRevB.109.155426.
- [9] H. Mustafa, C. Nnokwe, G. Ye, M. Fang, S. Chaudhary, J.-A. Yan, K. Wu, C. J. Cunningham, C. M. Hemesath, A. J. Stollenwerk, et al., Origin of Large Effective Phonon Magnetic Moments in Monolayer MoS₂, ACS nano, (2025). doi:10.1021/acsnano.4c18906.
- [10] D. Lujan, J. Choe, S. Chaudhary, G. Ye, C. Nnokwe, M. Rodriguez-Vega, J. He, F. Y. Gao, T. N. Nunley, E. Baldini, et al., Spin-orbit exciton-induced phonon chirality in a quantum magnet, Proceedings of the National Academy of Sciences 121, e2304360121 (2024). doi: 10.1073/pnas.2304360121.
- [11] F. Wu, S. Bao, J. Zhou, Y. Wang, J. Sun, J. Wen, Y. Wan, and Q. Zhang, Fluctuation-enhanced phonon magnetic moments in a polar antiferromagnet, Nature Physics 19, 1868 (2023). doi: 10.1038/s41567-023-02210-4.

- [12] F. Wu, J. Zhou, S. Bao, L. Li, J. Wen, Y. Wan, and Q. Zhang, Magnetic switching of phonon angular momentum in a ferrimagnetic insulator, Phys. Rev. Lett. 134, 236701 (2025). doi: 10.1103/gcgl-9sbb.
- [13] M. Che, J. Liang, Y. Cui, H. Li, B. Lu, W. Sang, X. Li, X. Dong, L. Zhao, S. Zhang, T. Sun, W. Jiang, E. Liu, F. Jin, T. Zhang, and L. Yang, Magnetic Order Induced Chiral Phonons in a Ferromagnetic Weyl Semimetal, Phys. Rev. Lett. 134, 196906 (2025). doi:10.1103/PhysRevLett.134.196906.
- [14] H. Ning, T. Luo, B. Ilyas, E. V. Boström, J. Park, J. Kim, J.-G. Park, D. M. Juraschek, A. Rubio, and N. Gedik, *Spontaneous emergence of phonon angular momentum through hybridization with magnons*, arXiv preprint arXiv:2410.10693, (2024). doi:10.48550/arXiv.2410.10693.
- [15] F. G. Hernandez, A. Baydin, S. Chaudhary, F. Tay, I. Katayama, J. Takeda, H. Nojiri, A. K. Okazaki, P. H. Rappl, E. Abramof, et al., Observation of interplay between phonon chirality and electronic band topology, Science advances 9, eadj4074 (2023). doi:10.1126/sciadv.adj4074.
- [16] M. Basini, M. Pancaldi, B. Wehinger, M. Udina, V. Unikandanunni, T. Tadano, M. C. Hoffmann, A. V. Balatsky, and S. Bonetti, *Terahertz electric-field-driven dynamical multiferroicity in SrTiO*₃, Nature, (2024). doi:10.1038/s41586-024-07175-9.
- [17] J. Luo, T. Lin, J. Zhang, X. Chen, E. R. Blackert, R. Xu, B. I. Yakobson, and H. Zhu, *Large effective magnetic fields from chiral phonons in rare-earth halides*, Science **382**, 698 (2023). doi:https://doi.org/10.1126/science.adi9601.
- [18] C. S. Davies, F. G. N. Fennema, A. Tsukamoto, I. Razdolski, A. V. Kimel, and A. Kirilyuk, *Phononic switching of magnetization by the ultrafast Barnett effect*, Nature **628**, 540 (2024). doi:10.1038/s41586-024-07200-x.
- [19] D. M. Juraschek, M. Fechner, A. V. Balatsky, and N. A. Spaldin, *Dynamical multiferroic-ity*, Physical Review Materials 1, 014401 (2017). doi:10.1103/PhysRevMaterials.1.014401.
- [20] F. Giustino, *Electron-phonon interactions from first principles*, Reviews of Modern Physics 89, 015003 (2017). doi:10.1103/RevModPhys.89.015003.
- [21] N. Shabala and R. M. Geilhufe, *Phonon Inverse Faraday Effect from Electron-Phonon Coupling*, Phys. Rev. Lett. 133, 266702 (2024). doi:10.1103/PhysRevLett.133.266702.
- [22] X. Gonze and C. Lee, Dynamical matrices, Born effective charges, dielectric permittivity tensors, and interatomic force constants from density-functional perturbation theory, Phys. Rev. B 55, 10355 (1997). doi:10.1103/PhysRevB.55.10355.
- [23] P. Ghosez, J.-P. Michenaud, and X. Gonze, *Dynamical atomic charges: The case of* ABO₃ compounds, Phys. Rev. B **58**, 6224 (1998). doi:10.1103/PhysRevB.58.6224.
- [24] C. A. Gonano, R. E. Zich, and M. Mussetta, *Definition for polarization P and magnetization M fully consistent with Maxwell's equations*, Progress In Electromagnetics Research B **64**, 83 (2015). doi:10.2528/PIERB15100606.
- [25] D. M. Juraschek and N. A. Spaldin, *Orbital magnetic moments of phonons*, Phys. Rev. Mater. 3, 064405 (2019). doi:10.1103/PhysRevMaterials.3.064405.
- [26] M. Freiser, A survey of magnetooptic effects, IEEE Transactions on magnetics 4, 152 (1968).

- [27] S. Liebes and P. Franken, Magnetic Moment of the Proton in Units of the Bohr Magneton; the Magnetic Moment of the Electron, Phys. Rev. 116, 633 (1959). doi:10.1103/PhysRev. 116.633.
- [28] L. Klebl, A. Schobert, M. Eckstein, G. Sangiovanni, A. V. Balatsky, and T. O. Wehling, *Ultrafast Pseudomagnetic Fields from Electron-Nuclear Quantum Geometry*, Phys. Rev. Lett. 134, 016705 (2025). doi:10.1103/PhysRevLett.134.016705.
- [29] Y. Ren, C. Xiao, D. Saparov, and Q. Niu, Phonon magnetic moment from electronic topological magnetization, Phys. Rev. Lett. 127, 186403 (2021). doi:10.1103/PhysRevLett.127. 186403.
- [30] S. Chaudhary, D. M. Juraschek, M. Rodriguez-Vega, and G. A. Fiete, *Giant effective magnetic moments of chiral phonons from orbit-lattice coupling*, Phys. Rev. B **110**, 094401 (2024). doi: 10.1103/PhysRevB.110.094401.
- [31] J. Fransson, *Chiral phonon induced spin polarization*, Physical Review Research 5, L022039 (2023). doi:10.1103/PhysRevResearch.5.L022039.
- [32] W. Chen, X.-W. Zhang, Y. Su, T. Cao, D. Xiao, and S.-Z. Lin, *Gauge theory of giant phonon magnetic moment in doped Dirac semimetals*, Physical Review B 111, 035126 (2025). doi: 10.1103/PhysRevB.111.035126.
- [33] R. M. Geilhufe, Dynamic electron-phonon and spin-phonon interactions due to inertia, Physical Review Research 4, L012004 (2022). doi:10.1103/PhysRevResearch.4.L012004.
- [34] T. Oka and S. Kitamura, Floquet engineering of quantum materials, Annual Review of Condensed Matter Physics 10, 387 (2019). doi:10.1146/annurev-conmatphys-031218-013423.
- [35] J. P. van der Ziel, P. S. Pershan, and L. D. Malmstrom, *Optically-Induced Magnetization Resulting from the Inverse Faraday Effect*, Phys. Rev. Lett. **15**, 190 (1965). doi:10.1103/PhysRevLett.15.190.
- [36] P. Pershan, J. Van der Ziel, and L. Malmstrom, *Theoretical discussion of the inverse Faraday effect, Raman scattering, and related phenomena*, Physical review 143, 574 (1966). doi: 10.1103/PhysRev.143.574.
- [37] D. Popova, *Microscopic description of the inverse Faraday effect at subpicosecond time scales.* PhD thesis, Aachen, Techn. Hochsch., Diss., 2013, 2014.
- [38] L. Zhang and Q. Niu, Angular Momentum of Phonons and the Einstein—de Haas Effect, Phys. Rev. Lett. 112, 085503 (2014). doi:10.1103/PhysRevLett.112.085503.
- [39] D. J. Griffiths and D. F. Schroeter, *Introduction to quantum mechanics* (Cambridge university press, 2018).
- [40] K. Van Benthem, C. Elsässer, and R. French, *Bulk electronic structure of SrTiO 3: Experiment and theory*, Journal of applied physics **90**, 6156 (2001). doi:10.1063/1.1415766.
- [41] J.-J. Zhou, O. Hellman, and M. Bernardi, Electron-Phonon Scattering in the Presence of Soft Modes and Electron Mobility in SrTiO₃ Perovskite from First Principles, Phys. Rev. Lett. 121, 226603 (2018). doi:10.1103/PhysRevLett.121.226603.
- [42] M. N. Gastiasoro, M. E. Temperini, P. Barone, and J. Lorenzana, *Generalized Rashba electron-phonon coupling and superconductivity in strontium titanate*, Phys. Rev. Res. 5, 023177 (2023). doi:10.1103/PhysRevResearch.5.023177.

- [43] F. Caruso and M. Zacharias, *Quantum theory of light-driven coherent lattice dynamics*, Phys. Rev. B **107**, 054102 (2023). doi:10.1103/PhysRevB.107.054102.
- [44] R. Merlin, Unraveling the effect of circularly polarized light on reciprocal media: Breaking time reversal symmetry with non-Maxwellian magnetic-esque fields, Phys. Rev. B 110, 094312 (2024). doi:10.1103/PhysRevB.110.094312.
- [45] R. Merlin, Magnetophononics and the chiral phonon misnomer, PNAS nexus 4, pgaf002 (2025). doi:10.1093/pnasnexus/pgaf002.
- [46] D. J. Griffiths, Introduction to electrodynamics (Cambridge University Press, 2023).
- [47] K. S. Novoselov, A. K. Geim, S. V. Morozov, D. Jiang, M. I. Katsnelson, I. V. Grigorieva, S. V. Dubonos, and A. A. Firsov, *Two-dimensional gas of massless Dirac fermions in graphene*, nature 438, 197 (2005). doi:10.1038/nature04233.
- [48] R. M. Geilhufe and A. V. Balatsky, Dirac Materials (In preparation, 2025).
- [49] F. D. M. Haldane, Model for a Quantum Hall Effect without Landau Levels: Condensed-Matter Realization of the "Parity Anomaly", Phys. Rev. Lett. 61, 2015 (1988). doi:10.1103/PhysRevLett.61.2015.
- [50] Z. Qiao, S. A. Yang, W. Feng, W.-K. Tse, J. Ding, Y. Yao, J. Wang, and Q. Niu, *Quantum anomalous Hall effect in graphene from Rashba and exchange effects*, Phys. Rev. B 82, 161414 (2010). doi:10.1103/PhysRevB.82.161414.
- [51] Z. Qiao, W. Ren, H. Chen, L. Bellaiche, Z. Zhang, A. MacDonald, and Q. Niu, *Quantum anomalous Hall effect in graphene proximity coupled to an antiferromagnetic insulator*, Physical Rev. Lett. 112, 116404 (2014). doi:10.1103/PhysRevLett.112.116404.
- [52] A. Manchon, H. C. Koo, J. Nitta, S. M. Frolov, and R. A. Duine, *New perspectives for Rashba spin-orbit coupling*, Nature materials 14, 871 (2015). doi:10.1038/nmat4360.
- [53] H. Vogt, Refined treatment of the model of linearly coupled anharmonic oscillators and its application to the temperature dependence of the zone-center soft-mode frequencies of KTaO₃ and SrTiO₃, Phys. Rev. B **51**, 8046 (1995). doi:10.1103/PhysRevB.51.8046.
- [54] Y. Claveau, B. Arnaud, and S. Di Matteo, Mean-field solution of the Hubbard model: the magnetic phase diagram, European Journal of Physics 35, 035023 (2014). doi:10.1088/0143-0807/35/3/035023.
- [55] C. Kittel, Introduction to solid state physics (John Wiley & Sons, 2005).
- [56] O. Yaniv and D. M. Juraschek, *Multicolor phonon excitation in terahertz cavities*, arXiv preprint arXiv:2504.03323, (2025). doi:10.48550/arXiv.2504.03323.